THE ASTRONOMICAL JOURNAL, 121:1915–1926, 2001 April

3C 236: RADIO SOURCE, INTERRUPTED?

CHRISTOPHER P. O'DEA, ANTON M. KOEKEMOER, STEFI A. BAUM, WILLIAM B. SPARKS, ANDRÉ R. MARTEL, MARK G. ALLEN, AND FERDINANDO D. MACCHETTO
Space Telescope Science Institute,[1] 3700 San Martin Drive, Baltimore, MD 21218

AND

GEORGE K. MILEY
Sterrewacht Leiden, Postbus 9315, NL-2300 RA Leiden, Netherlands
Received 2000 October 13; accepted 2000 December 20

ABSTRACT

We present new *Hubble Space Telescope* Space Telescope Imaging Spectrograph MAMA near-UV images and archival Wide Field Planetary Camera 2 (WFPC2) *V*- and *R*-band images that reveal the presence of four star-forming regions in an arc along the edge of the dust lane in the giant (4 Mpc) radio galaxy 3C 236. Two of the star-forming regions are relatively young, with ages of order $\sim 10^7$ yr, while the other two are older, with ages of order $\sim 10^8$–10^9 yr, which is comparable to the estimated age of the giant radio source. Based on dynamical and spectral aging arguments, we suggest that the fuel supply to the active galactic nucleus (AGN) was interrupted for $\sim 10^7$ yr and has now been restored, resulting in the formation of the inner 2 kpc–scale radio source. This timescale is similar to that of the age of the youngest of the star-forming regions. We suggest that the transport of gas in the disk is nonsteady and that this produces the multiple episodes of star formation in the disk, as well as the multiple epochs of radio source activity. If the inner radio source and the youngest star-forming region are related by the same event of gas transport, the gas must be transported from the hundreds of parsec scale to the subparsec scale on a timescale of $\sim 10^7$ yr, which is similar to the dynamical timescale of the gas on the hundreds of parsec scale.

Key words: galaxies: active — galaxies: individual (3C 236) — galaxies: jets — galaxies: starburst

1. INTRODUCTION

3C 236 is a powerful classical double radio galaxy at relatively low redshift ($z = 0.1$) (Willis, Strom, & Wilson 1974; Barthel et al. 1985; Schilizzi et al. 2001). Its angular size of 40′ corresponds to a projected linear size of 4 Mpc (possibly 4.5 Mpc deprojected; Schilizzi et al. 2001), making it the largest known radio galaxy and even one of the largest known objects in the universe.[2] There are no large-scale radio jets detected in this source. The bright lobes do not connect to the core; however, at low frequencies faint and diffuse bridges are seen (Mack et al. 1997; Waldram & Riley 1993). The nuclear radio source appears to be a small classical double source with an extent of 2 kpc and thus resembles a compact steep spectrum[3] radio source (Fomalont, Miley, & Bridle 1979; Barthel et al. 1985). Van Gorkom et al. (1989) detected the 21 cm line of H I in absorption against the nuclear radio source (this has since been imaged with *VLBI* by Conway 1999). One of the most remarkable features of 3C 236 is the alignment of the inner 2 kpc component with the overall 4 Mpc source structure to within a few degrees (Fomalont & Miley 1975), implying that the nuclear activity axis remains constant over times considerably in excess of 10^7 yr. The observed constancy in direction was one of the earliest indications that rotating black holes power extragalactic radio sources.

The presence of the 2 kpc radio source inside the 4 Mpc radio source suggests that 3C 236 is a member of the class of "double-double" radio sources (see, e.g., Schoenmakers et al. 1999, 2000a, 2000b; Kaiser, Schoenmakers & Röttgering 2000; Lara et al. 1999). Baum et al. (1990) have suggested that these sources are produced when (1) the radio activity is renewed after a period of dormancy so that the smaller and younger source is propagating outward amidst the relic of the previous epoch of activity and/or (2) the radio activity is temporarily interrupted, perhaps by "smothering" of the radio source by infall of gas.[4] In the latter case the nuclear jets must propagate outward though the infalling dense gas and reestablish a connection to the lobes. Hooda, Mangalam, & Wiita (1994) have presented numerical simulations that show that jets with low Mach numbers ($M < 3$) may "stall" because of an instability (even if the jet is still being continuously fed by the nucleus). The stalled jet creates a new hot spot within the lobe of the source that then continues to propagate outward.

Martel et al. (1999) presented a *Hubble Space Telescope* Wide Field Planetary Camera 2 (*HST* WFPC2) image in the broad red (F702W) filter of the host galaxy of 3C 236. They show that the galaxy contains a broad dust lane and circumnuclear knots of emission. The properties of the dust are discussed further by De Koff et al. (2000). In this paper

[1] Operated by the Association of Universities for Research in Astronomy, Inc., under contract NAS 5-26555 with the National Aeronautics and Space Administration.

[2] We adopt a Hubble constant of $H_0 = 75$ km s^{-1} Mpc^{-1} and a deceleration parameter of $q_0 = 0.1$, and at the redshift of 3C 236 ($z = 0.10050$) the scale is 1.68 kpc arcsec^{-1}.

[3] See O'Dea (1998) for a review of compact steep spectrum and GHz peaked spectrum radio sources.

[4] Christiansen (1973) has discussed repetitive activity in the context of plasma cloud models, and Bridle, Perley, & Henriksen (1986) have discussed a restarting jet model for 3C 219.

we present *HST* WFPC2 *V*-band (F555W) and Space Telescope Imaging Spectrograph (STIS) near-ultraviolet (NUV) MAMA near-UV images that show that these knots are very blue and are likely to be young star clusters. We discuss the implications of the star formation for the fueling and life cycle of the radio activity.

2. *HST* WFPC2 and STIS OBSERVATIONS

The *HST* observations were obtained as part of a snapshot survey of the 3CR sample by Sparks and collaborators (e.g., De Koff et al. 1996; McCarthy et al. 1997; Martel et al. 1999). 3C 236 was observed on the PC of WFPC2 (Trauger et al. 1994). The F555W and F702W data were reduced as described by Martel et al. (1999). The STScI calibration pipeline was rerun using updated reference files. Cosmic rays were removed by combining both images with the CRREJ task in the STSDAS package in IRAF. The STIS NUV MAMA (Kimble et al. 1998) images were reduced as described by Allen et al. (2001). Again the images were run though the STScI calibration pipeline using the best available reference files. The parameters of the observations are given in Table 1. Our STIS NUV MAMA image is present-

TABLE 1

JOURNAL OF *HST* OBSERVATIONS

Date	Program ID	Instrument	Filter	Time (s)
1995 May 7.....	5476	WFPC2 PC1	F702W	4 × 140
1996 Jun 12.....	6348	WFPC2 PC1	F555W	2 × 300
1999 Jan 3	8275	STIS NUV MAMA	F25SRF2	1440

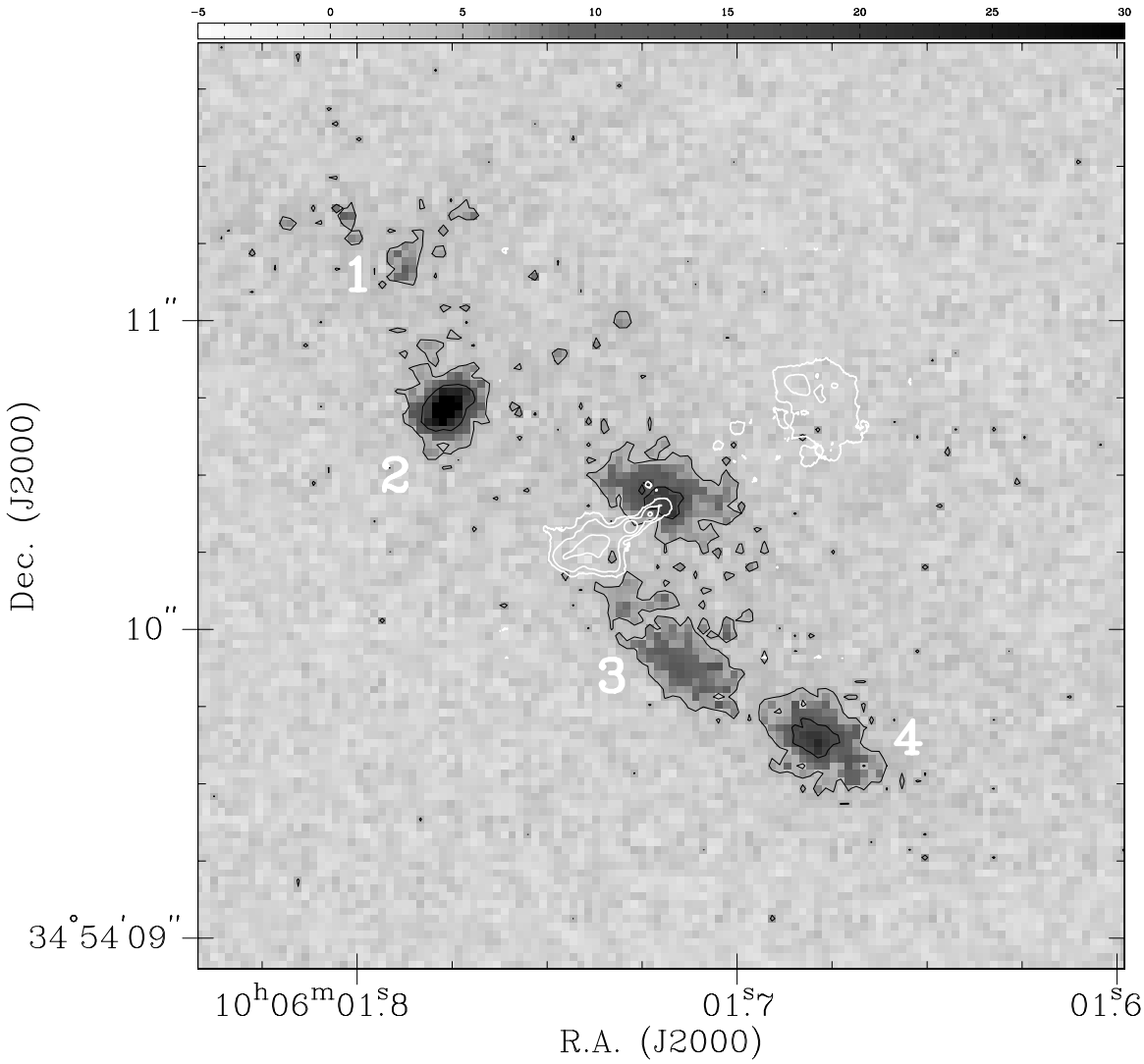

FIG. 1.—3C 236. Overlay of radio source contours (global *VLBI* 1.66 GHz image from Schilizzi et al. 2001) on our STIS near-UV image (*gray scale*). The four near-UV extranuclear features are labeled.

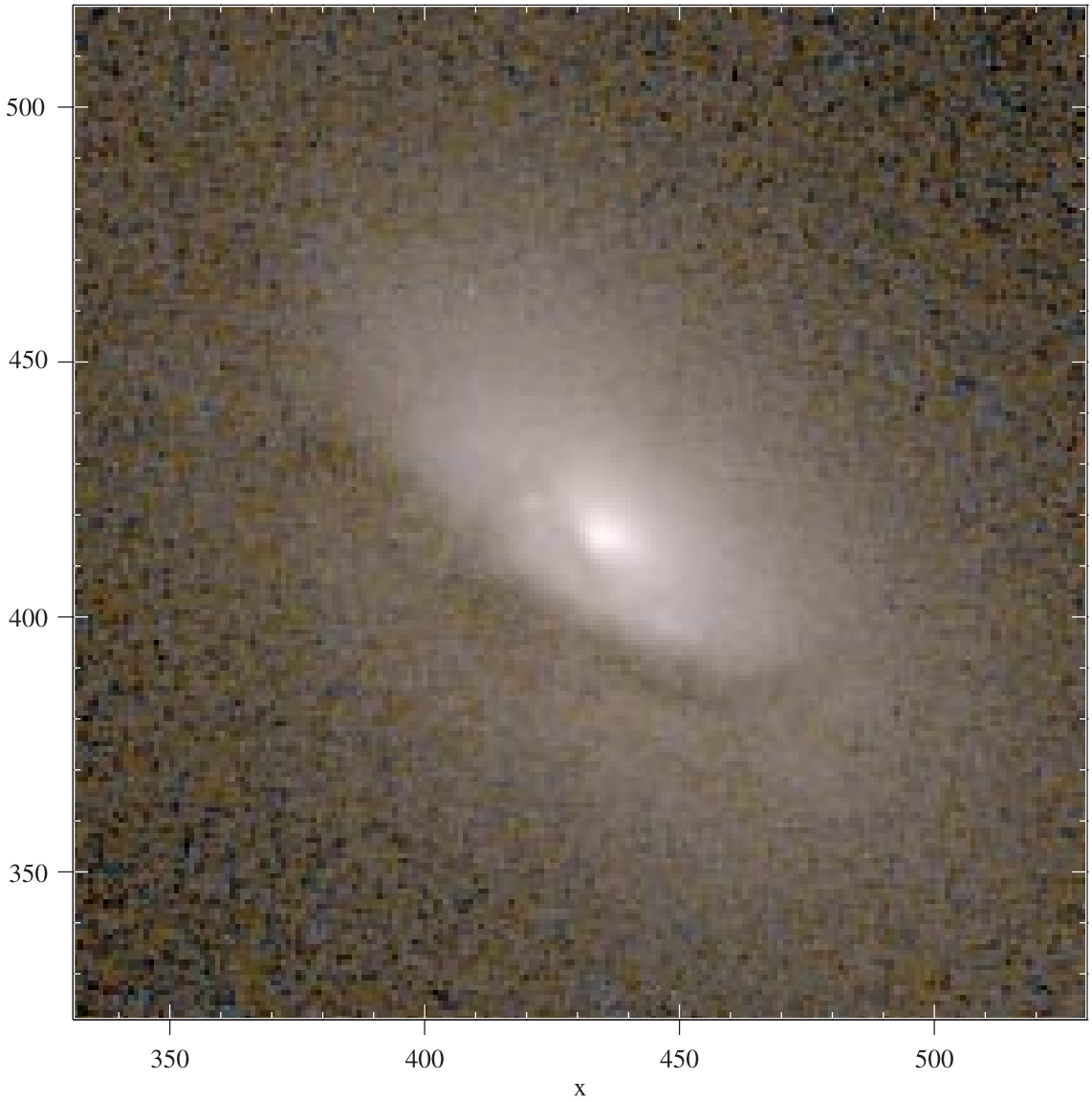

FIG. 2.—Three-color image of 3C 236, showing the STIS NUV MAMA image (*blue*), the WFPC2 F555W image (*green*), and the WFPC2/F702W image (*red*). Note in particular the presence of the extended dust lane to the south and southeast of the nucleus, as well as the more compact "disk" of obscuration closer to the nucleus at position angle $\sim 30°$.

ed in Figure 1 and a three-color image created by combining the STIS and WFPC2 data is shown in Figure 2.

3. RESULTS

Our main new observational result is the detection of several very blue resolved knots on the eastern edge of the dust lane (Figs. 1 and 3). First, we set the stage by discussing the large-scale dust lane that extends across much of the galaxy along its major axis and the inner "disk" of dust. We then discuss the properties of the very blue knots that we have detected with STIS, including their colors, luminosities, and inferred star formation characteristics, and finally the relationship between the radio continuum emission and the optical-UV morphology of the galaxy.

3.1. *Large-Scale Dust Lane and Inner Dust Disk*

In the broadband images (e.g., Martel et al. 1999) there are significant signs of asymmetric obscuration by a system of dust lanes (with an overall P.A. $\simeq 55°$) across the galaxy. Figures 3 and 4 show the relationship of the blue knots to the dust lane. In particular, the F555W image (Fig. 3) clearly shows a deficit of galaxy continuum immediately south of the blue knots, relative to the continuum level at corresponding radial distances in the north. Asymmetric deficits in the underlying elliptical morphology are also evident to the east and northeast of the galaxy nucleus.

To investigate more quantitatively the extent and depth of the obscuration, we used the IRAF ELLIPSE task to fit a set of elliptical isophotes to the underlying continuum in the F702W image. This band should be less susceptible to obscuration than the F555W image and thereby better constrain the fit. We also imposed additional constraints on the fit, including fixing the center of the isophotes (thus their symmetry about the nucleus) and masking out obscured regions in order to minimize their impact on the fit. The parameters of the ellipse fit are shown in Figure 5.

In Figure 4 we show the residual image produced after fitting the elliptical model to the underlying *R*-band galaxy

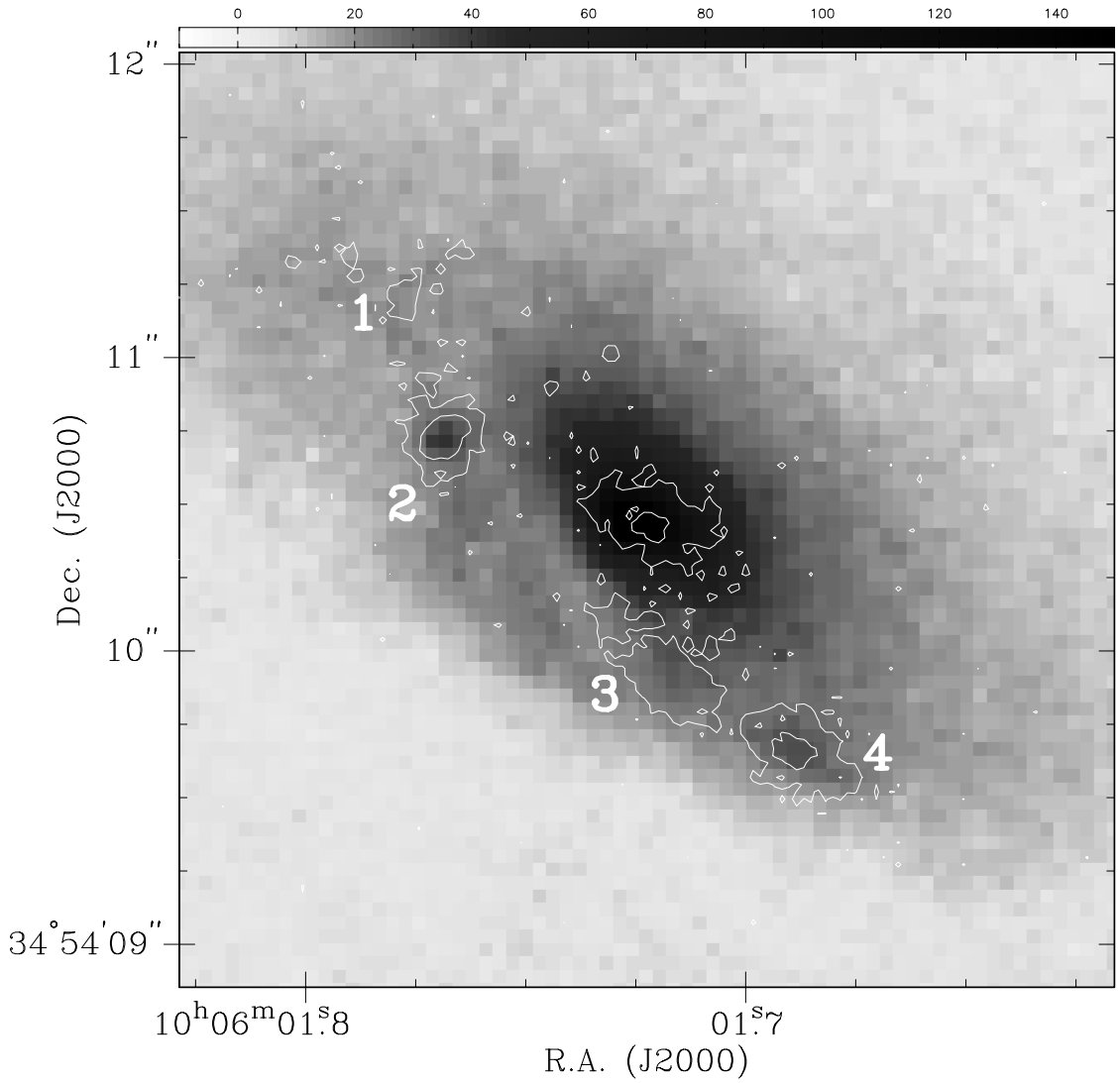

FIG. 3.—Overlay of STIS near-UV image (*contours*) of 3C 236 on WFPC2 F555W *V*-band image (*gray scale*)

continuum emission and subtracting this fit from the image. A large band of obscuration ~10 kpc in extent is clearly visible along the major axis of the galaxy. This can also be seen in the F555W − F702W color image of the galaxy (Fig. 6). The residual image also indicates substantial obscuration relatively close to the nucleus, along with additional arcs and loops of obscuration to the east and northeast of the nucleus. The implications of these features are discussed further in § 4.

Our color image (Fig. 2) shows what appears to be an inner narrow dust disk in projection at position angle P.A. ≃ 30°. (A hint of this is also seen in the absorption image of De Koff et al. 2000). The disk has a projected size of ≃0.″6 (1 kpc). This inner disk is about 5° from perpendicular to the inner radio source (P.A. ≃ 115°).

3.2. *Properties of the Near-UV Knots*

We detect a number of extended regions in our STIS NUV MAMA image (Figs. 3–4). There are four very blue regions located in an arc along the eastern edge of the dust lane at a distance of ~0.″5 (800 pc) from the nucleus. The regions are resolved, with sizes ~0.″3 (500 pc). The properties of the knots are given in Table 2 (calibrated in the *HST* VEGAMAG system, where the magnitude of Vega in the WFPC2 filters is defined to be zero). At the redshift of 3C 236 ($z = 0.1005$) there are no bright emission lines present in our F25SRF2 filter. The knots are located on the edge of the dust lane and are not related to the radio source or to an ionization cone. The most sensible explanation for the knots is that they are regions of recent and/or current star formation.

We compare the measured properties of the blue continuum with a set of stellar population synthesis models (Bruzual & Charlot 1993; Charlot & Bruzual 2001) that have been *K*-corrected to the redshift of 3C 236 and calibrated in the *HST* VEGAMAG system, using our *HST* filter bandpass transmission curves. We find it preferable to retain our measured magnitudes in the VEGAMAG system and compare them with models that have also been calculated in this system rather than attempting to transform the magnitudes to other systems, such as the Johnson Cousins system, because uncertainties in the color terms can translate into errors of several tenths of a magnitude. The models are shown in Figure 7 and represent two scenarios for star formation: (1) a constant star formation rate (SFR), assuming an invariant initial mass function (IMF) and (2)

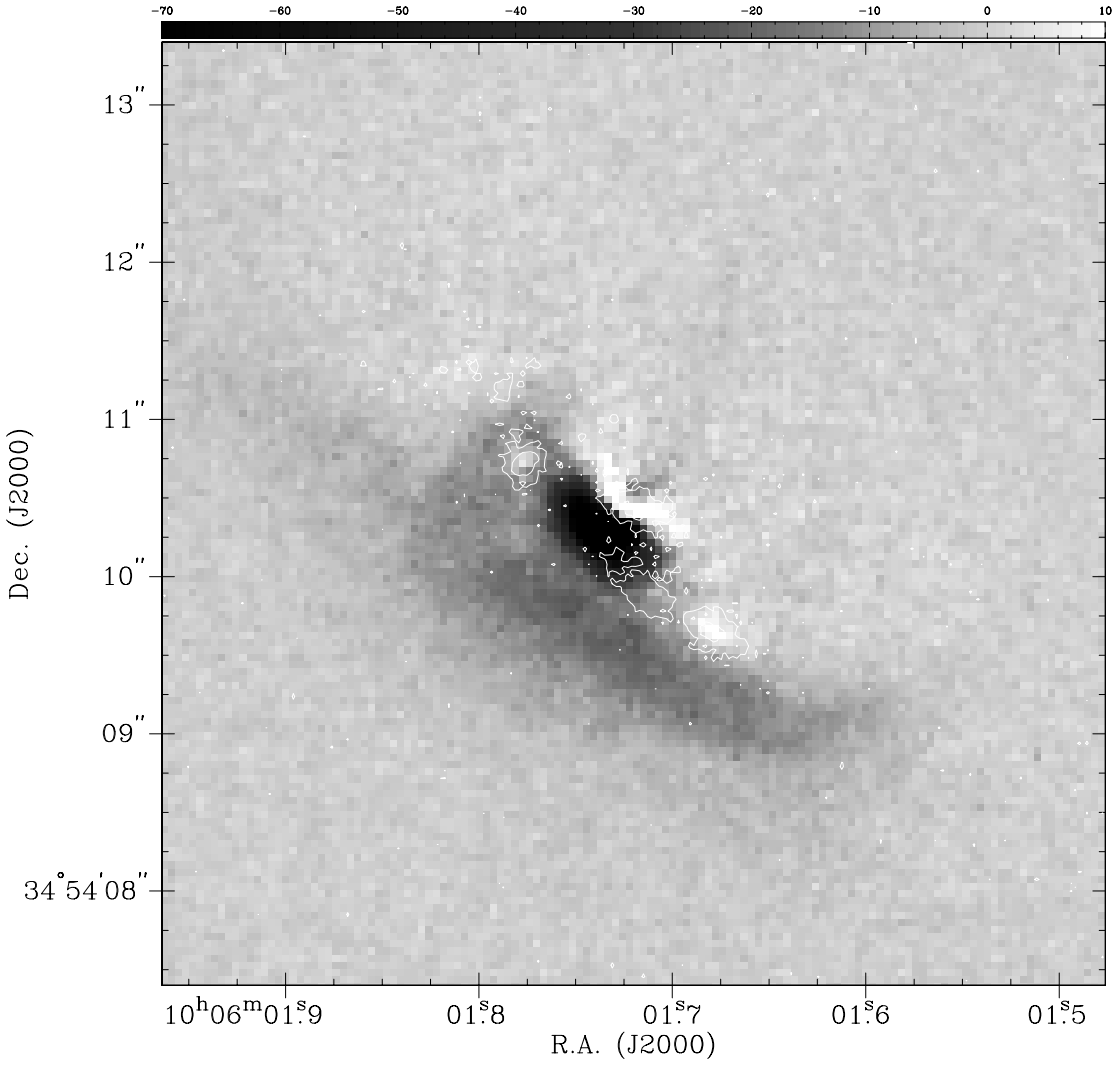

FIG. 4.—WFPC2 F702W (*R* band) image of 3C 236 with a fit to the elliptical isophotes subtracted to show the absorption due to the dust lane. Contours of the STIS near-UV image are superposed to show the location of the near-UV knots.

an instantaneous burst of star formation (or Simple Stellar Population, SSP). In each case we investigated two standard IMFs for which models were available, namely, Salpeter (1955) and Scalo (1986), with upper and lower mass cutoffs of 0.1 and 100 $M_\odot$, respectively. We also examined models of different metallicities, specifically, abundance $Z = Z_\odot$, 0.2 $Z_\odot$, and 0.02 $Z_\odot$ (where $Z_\odot$ is the solar abundance). Further details of the model parameterizations are described in Charlot & Bruzual (1991, 2001) and Bruzual & Charlot (1993). Having calculated *HST* colors and magnitudes for these various models, we note that the difference between the color evolution of $Z_\odot$ and 0.2 $Z_\odot$ models is minimal for the constant SFR models, thus for the purposes of clarity we plot only the 0.2 $Z_\odot$ models. For the SSP models, the color evolution is more sensitive to metallicity, but it is relatively insensitive to the choice of IMF, therefore the SSP models that we plot are for the Salpeter IMF only.

In Figure 7 we plot the evolution in color-age and color-color space of three population synthesis models with a

TABLE 2

BLUE REGIONS IN 3C 236

ID	ΔR.A. (arcsec)	Δdecl. (arcsec)	Size (arcsec)	$m_{F25SRF2}$(UV) (mag)	$m_{F555W}(V)$ (mag)	$m_{F702W}(R)$ (mag)	$m_{F25SRF2}-m_{F555W}$	$m_{F555W}-m_{F702W}$
1	+0.″8	+0.″8	0.″2	25.91 ± 0.07	26.74 ± 0.36	25.95 ± 0.23	−0.83 ± 0.43	0.79 ± 0.58
2	+0.″6	+0.″3	0.″3	23.89 ± 0.03	23.76 ± 0.08	24.05 ± 0.09	0.13 ± 0.11	−0.29 ± 0.17
3	−0.″1	−0.″3	0.″4 × 0.″2	24.04 ± 0.03	26.44 ± 0.30	26.70 ± 0.34	−1.40 ± 0.34	−0.26 ± 0.64
4	−0.″4	−0.″5	0.″3 × 0.″2	23.91 ± 0.03	23.12 ± 0.06	22.87 ± 0.05	0.79 ± 0.09	0.25 ± 0.11
Nuc.....	0	0	...	23.88 ± 0.03	20.93 ± 0.02	20.19 ± 0.01	2.95 ± 0.05	0.74 ± 0.04

NOTE.—For each object, the offsets in right ascension and declination are given in arcseconds relative to the continuum nucleus of the galaxy. The 1 σ uncertainties are derived from the count rate statistics.

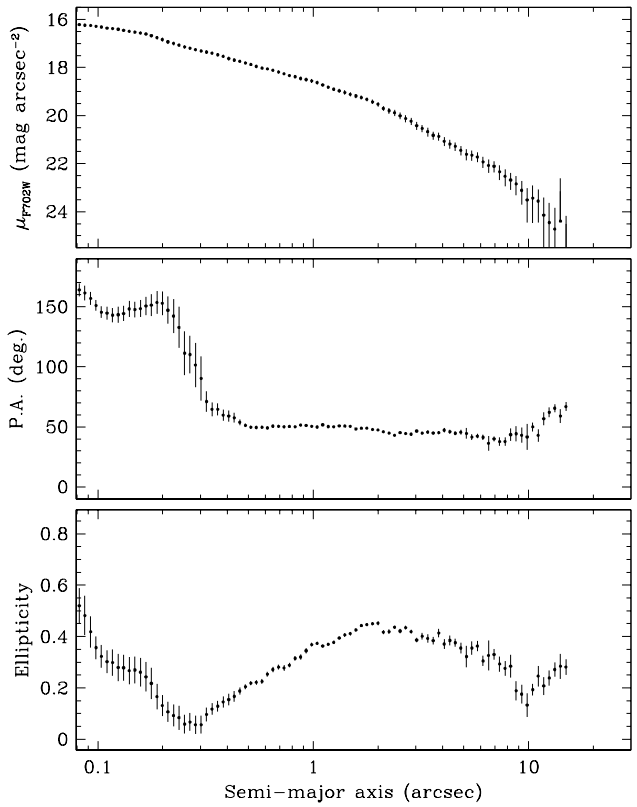

FIG. 5.—Results of the fit of elliptical isophotes to the WFPC2 F702W (R band) image of 3C 236: *top*, surface brightness profile; *middle*, position angle; *bottom*, ellipticity. We show the model parameters as a function of semimajor axis.

Salpeter IMF, metallicities of $Z_\odot$, 0.2 $Z_\odot$, and 0.02 $Z_\odot$, together with the observed blue clusters, as well as the surrounding galaxy and the nuclear region. The comparison suggests that the colors of the two bluest clusters are consistent with ages $\lesssim$5–10 Myr and metallicities above $\sim$0.2 $Z_\odot$, with ages of the two reddest of these clusters ranging up to a maximum of $\sim$100 Myr. The reddest of the four clusters is either much older ($\sim 10^9$ yr) with a mass $\sim 10^6\ M_\odot$ or otherwise is the same age as the other three but has higher extinction and/or a metallicity significantly above solar (however, this cluster is fainter than the other three and its properties are not as well constrained). In § 4 we discuss in further detail the implications of the measured properties of the blue continuum regions for various physical mechanisms that can be responsible for triggering the star formation.

In Table 3 we present the inferred star formation parameters that are required to match the observed range of colors and integrated absolute magnitude of the extended blue continuum distribution, for the various star formation scenarios that we have described. For each model, we tabulate the upper and lower limits of the range of epochs in its evolution that reproduce our observed $m_{\rm F555W}-m_{\rm F702W}$ color, as well as the $m_{\rm F25SRF2}-m_{\rm F555\,W}$ color. For constant SFR models the SFR for each of the two epochs is obtained by matching the model to the $M_{\rm F555W}$ absolute magnitude. For the instantaneous burst models we tabulate the total mass of stars (an SFR is not physically meaningful in this case since the burst is represented by a delta function).

We point out that the inferred ages are all highly dependent on the measured colors and should therefore be interpreted as *upper limits* due to the likely presence of reddening across most of the field. For example, a decrease in the intrinsic $m_{\rm F25SRF2}-m_{\rm F555\,W}$ color by only a further 0.2 mag will yield ages as low as 6×10^7 yr for the continuous SFR models and $\sim 5\times10^6$ yr for the instantaneous burst models. In summary, although the exact ages are uncertain and are model dependent, we do find that the knots span a range in age, with two of the knots being significantly younger ($\lesssim$5–10 Myr) than the other two ($\sim$100 Myr).

3.3. *Comparison between the Radio and HST Images*

In Figures 6 and 8 we show an overlay of the global *VLBI* 1.66 GHz radio image (Schilizzi et al. 2001) superposed onto the *HST* WFPC2 F555W broadband and F555W − F702W color images. The registration between the two images was performed on the assumption that the

TABLE 3

STAR FORMATION PARAMETERS FOR THE BLUE KNOTS

ABUNDANCE ($Z_\odot$)	REGIONS 1 AND 3		REGIONS 2 AND 4	
	log (τ/yr)	SFR ($M_\odot$ yr^{-1})	log (τ/yr)	SFR ($M_\odot$yr^{-1})
Constant SFR Model				
1	7.0–7.5	3.1–1.7	8.0–9.0	2.1–0.8
0.2	7.1–7.7	2.5–1.5	8.0–9.0	1.7–0.6
0.02	7.3–7.8	2.1–1.4	8.2–9.5	1.0–0.4
Instantaneous Burst Model				
Abundance ($Z_\odot$)	log (τ/yr)	log ($M/M_\odot$)	log (τ/yr)	log ($M/M_\odot$)
1	6.6–7.3	8.5–9.3	7.1–8.0	8.5–9.3
0.2	6.4–7.2	8.3–9.3	7.3–8.8	8.3–9.3
0.02	6.4–6.9	8.8–9.3	7.5–8.2	8.8–9.3

NOTE.—The upper and lower limits of the timescale τ of each model correspond to the epochs in the model evolution that produce the observed range of $m_{\rm F25SRF2}-m_{\rm F555\,W}$ colors. For the constant SFR models, the tabulated SFR is that required to match the observed integrated magnitude of the knots. For the instantaneous burst models, we instead tabulate the total mass of stars since in this model all the star formation occurs at one instant in time. Further details are given in the text.

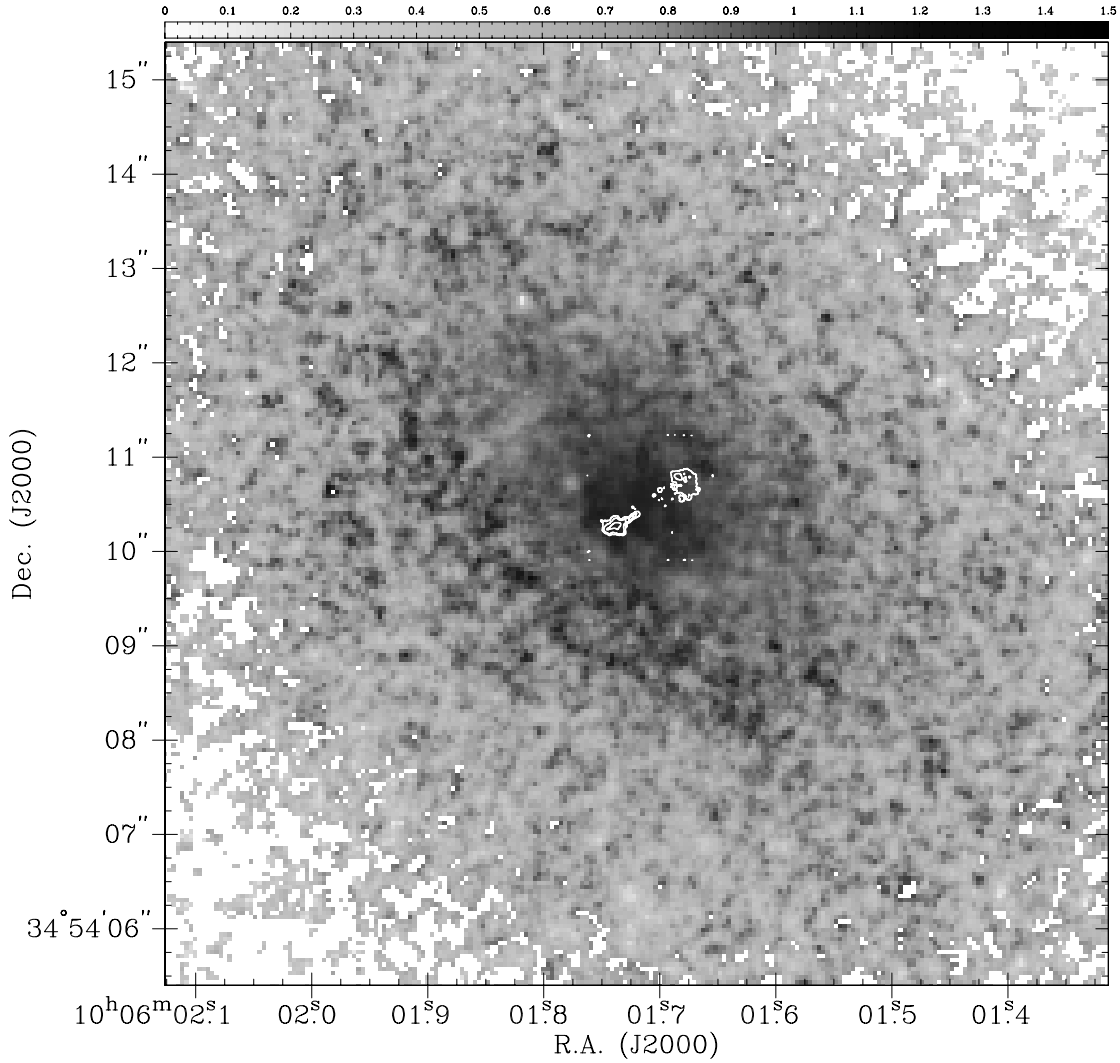

FIG. 6.— Overlay of radio image of 3C 236 (*left*) contours (global *VLBI* 1.66 GHz image from Schilizzi et al. 2001) on the WFPC2 F555W − F702W image (*gray scale*). The colors are calibrated in the *HST* VEGAMAG system.

position of the radio core is coincident with the optical nucleus of the galaxy in the F555W and F702W images (this is slightly different from the apparent registration in the Schilizzi et al. paper in which the radio core is identified with a STIS knot that is to the northeast of the broadband nucleus of the galaxy). Furthermore, there is no other strong correspondence between the kiloparsec-scale radio structure and the blue knots that we detect with STIS.

4. DISCUSSION

4.1. *Dust Lane and Inner Disk*

Gas acquired via cannibalism is expected to be smeared into a disk on a dynamical timescale $t_d \sim 10^8$ yr (e.g., Gunn 1979; Tubbs 1980). It will then precess around one of the preferred planes of the galaxy, dissipating angular momentum and finally settling into one of the preferred planes of the galaxy on the precession timescale $t_p \lesssim 10^9$ yr (Gunn 1979; Tubbs 1980; Tohline, Simonson, & Caldwell 1982; Habe & Ikeuchi 1985). The dissipation of angular momentum will also result in gas being transported inward toward the galaxy nucleus (e.g., Christodoulou & Tohline 1993). In 3C 236 the dust lane seems asymmetric and filamentary (De Koff et al. 2000; Fig. 4) and is misaligned with the inner disk, suggesting the lane is still "dynamically young." This indicates that the host galaxy has recently ($\lesssim 10^9$ yr) acquired gas from a companion.

3C 236 is in a very poor environment and is considered by Zirbel (1997) to have no obvious group members within 0.5 Mpc (based on a statistical correction for background contamination). The donor galaxy for the gas could have already been "eaten." However, we do detect a small candidate companion galaxy located at 10″.1 (17 kpc) from the nucleus along P.A. 20° in our WFPC2 images.

The mass of dust in the dust lane is estimated by De Koff et al. (2000) to be $\sim 10^7\ M_\odot$ based on both *HST* absorption maps and IRAS luminosities. The corresponding gas mass is $\sim 10^9\ M_\odot$ based on the standard gas-to-dust ratio. Thus, the dust lane appears to be very massive. The large amount of gas in the disk could supply fuel for a long time and would have allowed the radio galaxy to grow to its extremely large size. The relatively sparse environment of the galaxy may also be an important factor in producing the large radio source.

The absorption from the dust lane appears to be greater on the southeastern side of the galaxy, consistent with that side of the lane coming out of the galaxy toward us. This would imply that the northwestern radio jet is oriented

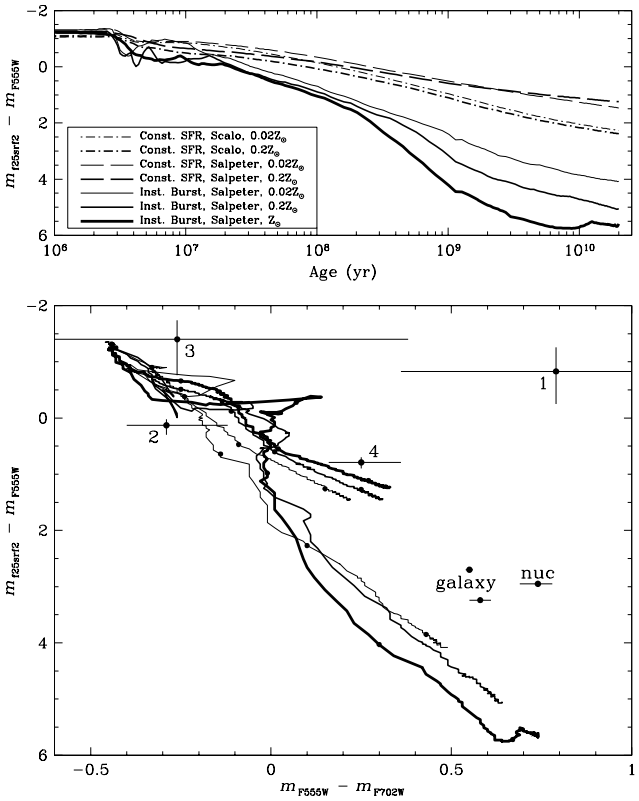

FIG. 7.—Blue knots in 3C 236. *Top*: $UV-V$ color (in VEGAMAGs) as a function of time for Bruzual and Charlot stellar population synthesis models for a range of parameters. We show evolution of models with both constant star formation, as well as an instantaneous burst, for metallicities of $Z_\odot$, 0.2 $Z_\odot$, and 0.02 $Z_\odot$, and for Scalo and Salpeter IMFs. *Bottom*: Evolution in color-magnitude space of three population synthesis models with a Salpeter IMF, metallicities of $Z_\odot$, 0.2 $Z_\odot$, and 0.02 $Z_\odot$, together with the observed colors of the blue clusters, as well as the colors of the surrounding galaxy and the nuclear region.

toward us and the southeastern jet is oriented away from us (as also inferred by Schilizzi et al. 2001 by using an image of De Koff et al.).

4.1.1. *Stability of the Alignments*

A summary of the relevant position angles are given in Table 4. The orientation of the large-scale (4 Mpc) radio source is 122.5° (Willis et al. 1974; Barthel et al. 1985). The overall orientation of the kiloparsec-scale central source is $\simeq$115—though there are wiggles in the kiloparsec-scale jet and departures from this overall orientation—and on the parsec scale the orientation of the jet is $\simeq$110° (Barthel et al. 1985; Schilizzi et al. 2001). Thus, over the lifetime of the radio source ($\sim 3 \times 10^8$ yr; § 4.3) and over a factor of 10^6 range in size, the jets remain aligned to within about 10°. The large- and small-scale radio sources are aligned to within a few degrees of perpendicular to the "inner" (1 kpc) dust disk, which has a projected major axis of $\simeq$30° but are poorly aligned with the perpendicular to the larger dust lane, which has a projected major axis of $\simeq$55°. Thus, the radio source axis is approximately perpendicular to the dust disk, as found in many radio galaxies (e.g., Kotanyi & Ekers 1979; De Koff et al. 1996; Verdoes et al. 1999).

TABLE 4

POSITION ANGLES

Feature	Position Angle (deg)	Reference
Kiloparsec-scale radio source	115	1, 2
Megaparsec-scale radio source.....	122	1, 3
Inner dust disk	30	4, 5
Outer dust lane	55	4, 5, 6
Host galaxy	45	4

REFERENCES.—(1) Barthel et al. 1985; (2) Schilizzi et al. 2001; (3) Willis et al. 1974; (4) this paper; (5) De Koff et al. 2000; (6) Martel et al. 1999.

The Bardeen-Petterson effect will cause the black hole to swing its rotation axis into alignment with the rotation axis of the disk of gas (on scales of hundreds to thousands of Schwarzschild radii), which is feeding it, and conversely will keep the spin axis of the inner disk aligned with the BH spin (e.g., Bardeen & Petterson 1975; Rees 1978). The timescale for alignment of the spin axes is uncertain but for typical parameters expected in the current paradigm will be in the range $t_{\rm align} \sim 10^6$–10^7 yr (Scheuer & Feiler 1996; Natarajan & Pringle 1998). This is much shorter than the radio galaxy lifetime and ensures that the jet will be ejected aligned with the angular momentum vector of the (large scale) accretion disk.

The combination of the long-term stability of the jet ejection axis and the alignment of the jets with the inferred rotation axis of the inner kiloparsec-scale dust disk suggests that the orientation of the inner dust disk has also been stable over the lifetime of the radio source. This is consistent with the inner dust disk being in a stable resonant orbit, most likely in either an oblate (Tohline et al. 1982) or triaxial galaxy (Merritt & de Zeeuw 1983). This also implies that the outer misaligned dust lane (which presumably feeds the disk) settles into the same preferred plane as the disk.

4.2. *Star-Forming Regions in the Dust Lane*

We note that the 3CR UV snapshot survey results suggest that a significant fraction ($\sim$30%) of powerful nearby radio galaxies show evidence for extended regions of star formation (Allen et al. 2001), consistent with early reports of blue colors in powerful radio galaxies (e.g., Smith & Heckman 1989; McNamara & O'Connell 1992; McNamara 1995). The lack of a direct relationship between the radio source and the starburst (in contrast to the more powerful objects at higher redshift) suggests that these are not jet-cocoon–induced starbursts, but may be infall induced. This suggests that (1) infall-induced starbursts are common in nearby radio galaxies and (2) the lifetimes of the starbursts are similar to that of the radio sources (which is luminosity dependent but is typically estimated to be 10^7–10^8 yr, e.g., Parma et al. 1999).

The analysis of the starburst colors suggests that the star formation has been triggered over timescales ranging from perhaps about 10^7–10^8 yr for the younger knots to about 10^8–10^9 yr for the older knots. The triggering mechanism of the starbursts is not known but may be due to (1) cloud-cloud collisions in adjacent orbits due to differential precession in the disk or (2) gas clouds continuing to fall into the disk.

The star formation in the disk suggests that gas continues to be transported into the nucleus, possibly fueling the nuclear activity. However the range of ages of the starbursts suggests that the transport of gas into the nucleus may be clumpy and sporadic, with different starbursts being triggered by different events of infall or transfer of gas. Thus, the existence of nonuniform transport of gas in the disk may

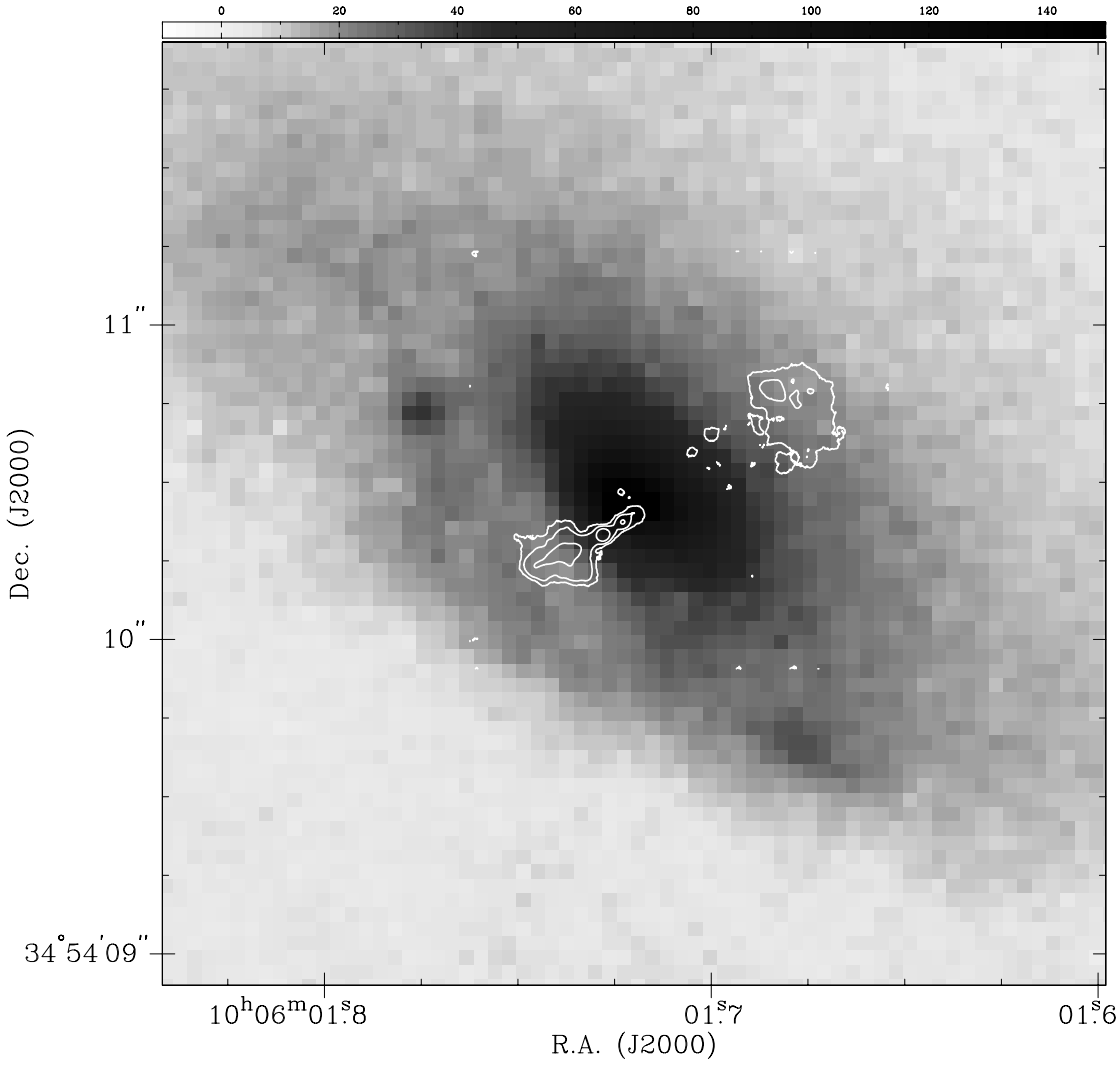

FIG. 8.—Overlay of radio image contours of 3C 236 (global *VLBI* 1.66 GHz image from Schilizzi et al. 2001) on the WFPC2 F555W image (*gray scale*)

be responsible for both (1) the range of ages of the star-forming regions and (2) the apparent episodic nature of the radio source.

4.3. *Relationship between the Starbursts and the Radio Source*

The large-scale source has a total projected linear size of about 4 Mpc. The projected length of the southeastern side of the source is about 24′ (2.4 Mpc). The minimum age of the large-scale source is then

$$t_{\rm min} \simeq 7.8 \times 10^6 \left(\frac{v_{\rm lobe}}{c}\right)^{-1} \ {\rm yr}\ , \qquad (1)$$

where $v_{\rm lobe}$ is the advance speed of the lobe. For a canonical expansion speed of $0.03c$ (e.g., Scheuer 1985; Alexander & Leahy 1987) the minimum age is 2.6×10^8 yr. The radio source age is similar to the dynamical timescale in the galaxy and the age estimates for the older starbursts, suggesting that the large-scale radio galaxy and the initiation of the starbursts are related by a common event, i.e., the infall of gas.

We note that the starbursts appear to be confined to the dust disk and are not associated with the small-scale radio source. Thus, there does not appear to have been any significant "jet-induced" star formation in this source. This is consistent with the hypothesis that the dense gas is mostly confined to the plane of the disk and avoids the radio source (which seems to be perpendicular to the dust disk).

Conway (1999) and Conway & Schilizzi (2001) present *VLBI* imaging of the H I absorption toward the inner radio source. He shows significant H I absorption toward the southeastern jet or lobe, but none toward the northwestern lobe. This is consistent with the southeastern jet being viewed through the dust lane, while the northwestern jet is in front of the dust lane. Conway (1999) suggests that there is evidence from the kinematics of the H I for a possible interaction between the southeastern jet or lobe and the H I gas. This interaction would explain the asymmetry in the kiloparsec-scale radio source (i.e., the southeastern side is brighter and shorter than the northwestern side). We note that such an interaction, if present, has not produced any detectable star formation.

4.4. *Relationship of the Small and Large Radio Sources*

Here we consider the possible relationships between the small-scale (2 kpc) and large-scale (4.5 Mpc) radio sources. The small source could be (1) brightness enhancements

(knots) in the inner part of the large-scale jet, (2) a young source that has resumed activity after a period of dormancy of the active nucleus, or (3) the location of the working surfaces of the jet due to infall of gas that has smothered the radio jet and temporarily interrupted the supply of energy to the lobes.

4.4.1. *Bright Inner Part of Continuous Jet*

The morphology of the small source argues against the first possibility. The small source does not resemble knots in the inner parts of jets. Instead, we see structures that look like lobes marking the ends of the jet. The spectral indices of the small source show a range of values extending to very steep spectra $\alpha \simeq -1$ (Schilizzi et al. 2001). These steep spectra are more consistent with those of radio lobes than with knots in jets, which tend to be $\alpha \simeq -0.65$ (e.g., Bridle & Perley 1984). Schilizzi et al. have suggested that the radio jet extends in a continuous fashion from the core to the lobes, based on faint emission seen in the low-frequency, low-resolution images. However, (1) an alternate explanation for the faint emission is that it is a low surface brightness cocoon or "bridge" and (2) in a continuous jet scenario there is still an unexplained sudden transition in the jet properties at the scale of the kiloparsec source. Thus, for the rest of the discussion we consider further only the second and third scenarios.

4.4.2. *Young Source*

If the central 2 kpc source is a young source, then its age is given by

$$t_{\min} \simeq 3.2 \times 10^3 \left(\frac{v_{\rm lobe}}{c}\right)^{-1} \text{ yr} , \qquad (2)$$

where for an advance speed of $v_{\rm lobe} = 0.03c$ the minimum age is 1.0×10^5 yr. This is much younger than the youngest of the star-forming regions in the dust lane. Note that a difference in the ages is to be expected since the star formation occurs on the kiloparsec scale and the jet is fed on the subparsec scale.

We assume that the steep spectra in the small source found by Schilizzi et al. indicate radiative aging of the electrons rather than an intrinsically steep electron spectrum. This implies that the dynamical age of the source is greater than its radiative age. For a given magnetic field, this gives an upper limit on the lobe advance speed $v_{\rm lobe} < l/t_{\rm rad}$, where l is the distance between the core and hot spot and $t_{\rm rad}$ is the electron radiative lifetime due to synchrotron and inverse Compton losses,

$$t_{\rm rad} \simeq 2.6 \times 10^4 \left\{\frac{B^{0.5}}{(B^2 + B_R^2)[(1+z)\nu]^{0.5}}\right\} \text{ yr} , \qquad (3)$$

where ν is the frequency (in hertz), B is the magnetic field in gauss, and $B_R = 4(1+z)$ is the equivalent magnetic field of the microwave background (e.g., van der Laan & Perola 1969). We plot the upper limit to the lobe expansion speed as a function of magnetic field strength, adopting a size of 1 kpc and a frequency of 5 GHz in Figure 9. At the equipartition magnetic field in the two lobes A and C of a few hundred microgauss the particle lifetime is $t_{\rm rad} \lesssim 10^5$ yr and the upper limit to the expansion velocity is a few percent of the speed of light.

In the young source scenario, the nucleus becomes dormant possibly for lack of fuel to the central engine, the jets cease, and the previously ejected jet material traverses the length of the source in the light travel time (assuming the jet bulk velocity is relativistic) shutting off the energy supply to the hot spots (e.g., Baum et al. 1990; Schoenmakers et al. 2000a, 2000b; Kaiser et al. 2000). We assume that the particles are accelerated primarily in the hot spots (perhaps by Fermi acceleration in the Mach disk; Blandford & Ostriker 1978; or by MHD turbulence; De Young 2001) and that the acceleration will cease when the jet no longer feeds the hot spot. Thus, the particle population will age once the hot spots are no longer fed. If the jet bulk velocity is relativistic, as commonly assumed in powerful classical doubles, then the jets will propagate to the hot spots in about 6×10^6 yr. Then, the ages of the youngest electrons in the lobe provides a constraint on the dormancy period of the nucleus. This assumes that the spectral aging estimates are dominated by the younger and brighter electron population (see also Jones, Ryu, & Engel 1999). This appears to be the case since the age estimated from spectral aging is significantly less than the dynamical age based on the likely lobe propagation velocity.

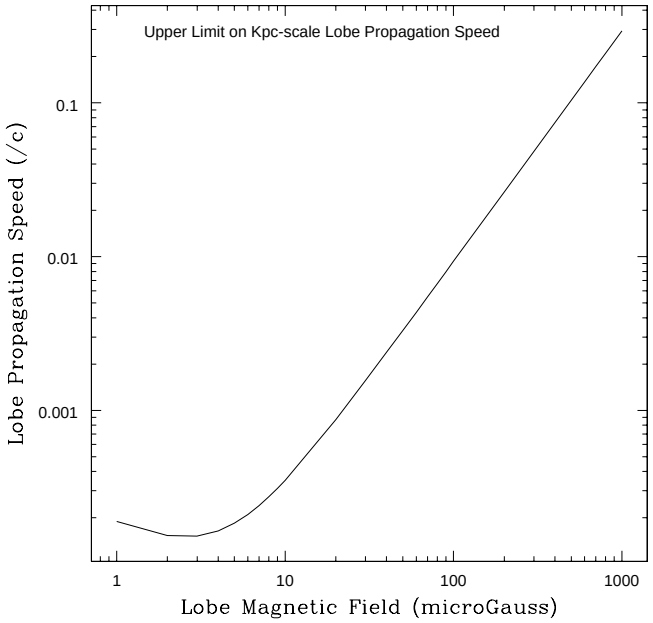

FIG. 9.— Plot of the upper limit on the lobe expansion velocity of the kiloparsec-scale radio source 3C 236 as a function of lobe magnetic field, assuming that the source age is given by the radiative loss time (eq. [3]). At the lobe equipartition magnetic field of a few hundred microgauss, the lobe expansion velocity is less than a few percent of the speed of light.

The dormancy period could be longer if (1) the acceleration continues for some timescale after the jet ceases to feed the hot spot, (2) the jet propagation to the lobes is significantly slower than light speed, or (3) the spectral aging estimates are in error (see, e.g., Tribble 1993; Rudnick, Katz-Stone, & Anderson 1994).

The radio spectral aging estimates from Mack et al. (1998) are consistent with ages for the electrons in the hot spots of order 1×10^7 yr. This would imply a dormancy period for the nucleus of $\gtrsim 1 \times 10^7$ yr. If this is the correct model, it would imply that even though the dust lane is present the flow of material to the nucleus is not continuous; instead it is clumpy and sporadic on timescales of $\sim 10^7$ yr. Alternately, there could be an additional factor responsible for the duty cycle of the central engine that is not directly related to the fuel supply (e.g., some property of

the magnetic field in the accretion disk that varies on timescales of $\sim 10^7$ yr).

4.4.3. *Interrupted Source*

In the third scenario, the nucleus is active continuously; however, dense gas clouds fall into the path of the radio jet and block the passage of both jets. The energy supply to the lobes is then cut off until the jets are able to burrow through the clouds and reestablish a connection to the lobes.

This scenario requires that both jets be cut off symmetrically. The existence of H I absorption toward the radio source and the evidence for possible interaction between the southeastern jet and the H I gas would support the interrupted-source scenario. However, there is no evidence for interaction of the northwestern lobe with ambient gas. In general, it seems that it would be more difficult to block *both* jets with infalling gas than it would be to simply shut off the fuel supply to the engine (i.e., no infall).

As in the previous scenario, the particles in the hot spots will age after the energy supply is cut off. In this scenario, the time during which the jets have been blocked, the age of the youngest electrons in the hot spots, and the age of the small source should all be similar, i.e., $\sim 10^7$ yr, adopting the spectral aging estimates of Mack et al. (1998). This age seems extremely long for such a compact source and would imply the existence of a cocoon of very steep spectrum emission—which has not been detected (Schilizzi et al. 2001).

Thus, in the interrupted source scenario the two jets have been blocked for about $\sim 10^7$ yr by dense gas. This requires (1) the presence of dense gas surrounding the jets (2) the age of the kiloparsec-scale source to be $\gtrsim 10^7$ yr. However, as we have argued above, there is no evidence that *both* jets have been blocked. At present, (1) the very old implied age for the compact radio source and the lack of very steep spectrum radio emission and (2) the lack of evidence for strong confinement of both jets by dense gas are problems for the scenario in which the radio source has been interrupted by infalling gas.

4.5. *Nonsteady Flow in the Disk?*

The fact that the dust lane is asymmetric, is filamentary, and is misaligned with the inner disk suggests that it is dynamically young. During this phase it is expected to be precessing around the preferred plane, dissipating angular momentum, and transporting gas inward to the nucleus through processes such as viscosity and cloud-cloud collisions (e.g., Shlosman, Begelman, & Frank 1990). The collisions of these clumps and filaments in the disk may well trigger the observed star formation. The range of estimated ages for the star-forming regions implies that the star formation is triggered over a range of timescales and is not based on a single event. Thus, the existence of the observed clumps and filaments in the dust lane, as well as the range of ages of the star formation regions, suggests that the transport of gas through the disk to the nucleus is clumpy and nonsteady.

As we have discussed, the properties of the inner 2 kpc radio source are consistent with a scenario in which the fuel supply to the nucleus was interrupted for $\sim 10^7$ yr and has now been restored. This apparent intermittancy in the fuel supply is evidence that the transport of fuel on the subparsec scale is also clumpy and nonsteady. The outflows in young stellar objects and Herbig-Haro objects also appear to show evidence for nonsteady fueling and repetitive activity (e.g., Reipurth, Raga, & Heathcote 1992; Bally & Devine 1994; Eisloffel & Mundt 1997). Thus, we suggest that the range of ages in the star-forming regions and the repetitive activity in the AGN in 3C 236 are both due to nonsteady transport of gas in the disk on their respective scales.

We note that a one-to-one correspondence in the age of the young inner radio source and the youngest starburst in the dust lane is not necessarily expected since the dynamical time on the hundreds of parsecs scale where the star formation occurs ($\sim 10^7$ yr) is longer than the dynamical timescale on the subparsec scale where the fueling of the AGN occurs. However, if the young radio source and the youngest star-forming region are both produced by the same "disturbance" propagating inward through the disk, then we can use the difference in the ages of the youngest starburst ($\sim 10^7$ yr) and the inner radio source ($\sim 10^5$ yr) to constrain the propagation time. Thus, in the context of this scenario, the time for the gas to be transported inward from the hundreds of parsec scale to the subparsec scale is no more than 10^7 yr, which is comparable to the dynamical time on the hundreds of parsec scale. If this is correct, it implies that nature is able to solve the angular momentum problem on these scales and that clumps of gas are transported inward on the dynamical timescale.

5. SUMMARY AND THE BIG PICTURE

We present *HST* WFPC2 *V*- and *R*-band images and STIS MAMA NUV images that reveal the presence of four star-forming regions in the dust lane in the giant (4 Mpc) radio galaxy 3C 236. The dust lane appears to be asymmetric and is misaligned with the inner disk, suggesting it is still dynamically young. The dust lane appears to be quite massive ($\sim 10^9\ M_\odot$; De Koff et al. 2000) and clumpy.

Two of the star-forming regions are relatively young, with ages of $\lesssim$5–10 Myr and metallicities above $\sim 0.2\ Z_\odot$, while the other two are older, with ages ranging up to a maximum of $\sim$100 Myr and $\sim 10^9$ yr. We note that the age of the giant radio source is likely to be $\sim 10^8$–10^9 yr. Thus, the star formation appears to be coeval with the radio source lifetime. The star formation and the radio source may both be the common result of infall of gas to the host galaxy.

We consider two hypotheses for the small kiloparsec-scale source in 3C 236: (1) It may be a young source ($\sim 10^5$ yr) that has resumed activity after a period of nuclear dormancy of about 10^7 yr (based on the spectral ages of the electrons in the radio lobes) and (2) it may be a continuously active source in which infalling gas has interrupted the jet flow to the lobes for a period of about 10^7 yr. Both the "young" and "interrupted" source scenarios require that energy is no longer being supplied to the hot spots. This should be tested with high-resolution radio observations of the hot spots. Currently, the rather old age required for the small source and the apparent lack of a mechanism for confining the radio source make the interrupted source hypothesis less appealing.

The simultaneous existence of the small and large radio source is consistent with repetitive activity in the nucleus on timescales of $\sim 10^7$ yr. The repetitive nuclear activity may be tied to time dependence in the infall of fuel on the same timescale. This timescale is similar to that of the ages of the younger of the star-forming knots. The range of ages of the star-forming regions implies repetitive triggering or fueling

of the star formation activity in the dust lane. Thus, there is evidence for nonsteady activity on both size scales in which clumps of gas are transported inward to the nucleus on the dynamical timescale.

We suggest that the transport of gas in the disk is nonsteady over a large range of size scales and that this produces the multiple episodes of star formation in the disk, as well as the multiple epochs of radio source activity.

We are grateful to Richard Schilizzi for sharing his results in advance of publication and Paul Wiita for helpful discussions. This work was based on observations made with the NASA/ESA *Hubble Space Telescope*, obtained from the data archive at the Space Telescope Science Institute. STScI is operated by the Association of Universities for Research in Astronomy, Inc., under NASA contract NAS 5-26555. This work was partially supported by STScI grant GO 08275.01-97A. This research made use of the NASA/IPAC Extragalactic Database (NED), which is operated by the Jet Propulsion Laboratory, California Institute of Technology, under contract with the National Aeronautics and Space Administration, and of NASA's Astrophysics Data System Abstract Service.

REFERENCES

Alexander, P., & Leahy, J. P. 1987, MNRAS, 225, 1
Allen, M. G., et al. 2001, in preparation
Bally, J., & Devine, D. 1994, ApJ, 428, L65
Bardeen, J. M., & Petterson, J. A. 1975, ApJ, 195, L65
Barthel, P. D., Schilizzi, R. T., Miley, G. K., Jägers, W. J., & Strom, R. G. 1985, A&A, 148, 243
Baum, S. A., O'Dea, C. P., Murphy, D. W., & de Bruyn, A. G. 1990, A&A, 232, 19
Blandford, R. D., & Ostriker, J. P. 1978, ApJ, 221, L29
Bridle, A. H., & Perley, R. A. 1984, ARA&A, 22, 319
Bridle, A. H., Perley, R. A., & Henriksen, R. 1986, AJ, 92, 534
Bruzual, A. G., & Charlot, S. 1993, ApJ, 405, 538
Charlot, S., & Bruzual, A. G. 1991, ApJ, 367, 126
———. 2001, in preparation
Christiansen, W. A. 1973, MNRAS, 164, 211
Christodoulou, D. M., & Tohline, J. E. 1993, ApJ, 403, 110
Conway, J. E. 1999, NewA Rev., 43, 509
Conway, J. E., & Schilizzi, R. T. 2001, in preparation
De Koff, S., Baum, S. A., Biretta, J., Golombek, D., Macchetto, F. D., McCarthy, P. J., Miley, G. K., & Sparks, W. B. 1996, ApJS, 107, 621
De Koff, S., et al. 2000, ApJS, 129, 33
De Young, D. S. 2001, in Particles and Fields in Radio Galaxies, ed. R. Laing & K. Blundell (San Francisco: ASP), in press
Eisloffel, J., & Mundt, R. 1997, AJ, 114, 280
Fomalont, E. B., & Miley, G. K. 1975, Nature, 257, 99
Fomalont, E. B., Miley, G. K., & Bridle, A. H. 1979, A&A, 76, 106
Gunn, J. E. 1979, in Active Galactic Nuclei, ed. C. Hazard & S. Mitton (Cambridge: Cambridge Univ. Press), 213
Habe, A., & Ikeuchi, S. 1985, ApJ, 289, 540
Hooda, J. S., Mangalam, A. V., & Wiita, P. 1994, ApJ, 423, 116
Jones, T. W., Ryu, D., & Engel, A. 1999, ApJ, 512, 105
Kaiser, C. R., Schoenmakers, A. P., & Röttgering, H. J. A. 2000, MNRAS, 315, 381
Kimble, R. A., et al. 1998, ApJ, 492, L83
Kotanyi, C., & Ekers, R. D. 1979, A&A, 73, L1
Lara, L., Márquez, I., Cotton, W. D., Feretti, L., Giovannini, G., Marcaide, J. M., & Venturi, T. 1999, A&A, 348, 699
Mack, K.-H., Klein, U., O'Dea, C. P., & Willis, A. G. 1997, A&AS, 123, 423
Mack, K.-H., Klein, U., O'Dea, C. P., Willis, A. G., & Saripalli, L. 1998, A&A, 329, 431
Martel, A. R., et al. 1999, ApJS, 122, 81
McCarthy, P. J., Miley, G. K., de Koff, S., Baum, S. A., Sparks, W. B., Golombek, D., Biretta, J., & Macchetto, F. 1997, ApJS, 112, 415
McNamara, B. R. 1995, ApJ, 443, 77
McNamara, B. R., & O'Connell, R. W. 1992, ApJ, 393, 579
Merritt, D., & De Zeeuw, T. 1983, ApJ, 267, L19
Natarajan, P., & Pringle, J. E. 1998, ApJ, 506, L97
O'Dea, C. P. 1998, PASP, 110, 493
Parma, P., Murgia, M., Morganti, R., Capetti, A., de Ruiter, H. R., & Fanti, R. 1999, A&A, 344, 7
Rees, M. J. 1978, Nature, 275, 516
Reipurth, B., Raga, A. C., & Heathcote, S. 1992, ApJ, 392, 145
Rudnick, L., Katz-Stone, D. M., & Anderson, M. C. 1994, ApJS, 90, 955
Salpeter, E. E. 1955, ApJ, 121, 161
Scalo, J. 1986, Fundam. Cosmic Phys. 11, 1
Scheuer, P. A. G. 1995, MNRAS, 277, 331
Scheuer, P. A. G., & Feiler, R. 1996, MNRAS, 282, 291
Schilizzi, R. T., Tian, W. W., Conway, J. E., Nan, R., Miley, G. K., Barthel, P. D., & Normandeau, M. 2001, A&A, in press
Schoenmakers, A. P., de Bruyn, A. G., Röttgering, H. J. A., & van der Laan, H. 1999, A&A, 341, 44
———. 2000a, MNRAS, 315, 395
Schoenmakers, A. P., de Bruyn, A. G., Röttgering, H. J. A., van der Laan, H., & Kaiser, C. R. 2000b, MNRAS, 315, 371
Shlosman, I., Begelman, M. C., & Frank, J. 1990, Nature, 345, 679
Smith, E. P., & Heckman, T. M. 1989, ApJ, 341, 658
Tohline, J. E., Simonson, G. F., & Caldwell, N. 1982, ApJ, 252, 92
Trauger, J. T., et al. 1994, ApJ, 435, L3
Tribble, P. C. 1993, MNRAS, 261, 57
Tubbs, A. D. 1980, ApJ, 241, 969
van der Laan, H., & Perola, G. C. 1969, A&A, 3, 468
van Gorkom, J. H., Knapp, G. R., Ekers, R. D., Ekers, D. D., Laing, R. A., & Polk, K. S. 1989, AJ, 97, 708
Verdoes Kleijn, G. A., Baum, S. A., de Zeeuw, P. T., & O'Dea, C. P. 1999, AJ, 118, 2592
Waldram, E. M., & Riley, J. M. 1993, MNRAS, 265, 853
Willis, A. G., Strom, R. G., & Wilson, A. S. 1974, Nature, 250, 625
Zirbel, E. L. 1997, ApJ, 476, 489